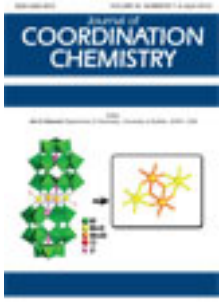

Journal of Coordination Chemistry
Publication details, including instructions for authors and subscription information:
http://www.tandfonline.com/loi/gcoo20

Noncentrosymmetry in new 2-methylpiperazinediium hexaaquazinc(II) bis(sulfate)

Houcine Naïli [a]

[a] Laboratoire de l'Etat Solide, Département de Chimie , Université de Sfax , BP 1171, 3000 Sfax , Tunisie

Published online: 13 Mar 2012.

To cite this article: Houcine Naïli (2012) Noncentrosymmetry in new 2-methylpiperazinediium hexaaquazinc(II) bis(sulfate), Journal of Coordination Chemistry, 65:7, 1178-1188, DOI: 10.1080/00958972.2012.669476

To link to this article: http://dx.doi.org/10.1080/00958972.2012.669476

Journal of Coordination Chemistry
Vol. 65, No. 7, 10 April 2012, 1178–1188

Noncentrosymmetry in new 2-methylpiperazinediium hexaaquazinc(II) bis(sulfate)

HOUCINE NAÏLI*

Laboratoire de l'Etat Solide, Département de Chimie,
Université de Sfax, BP 1171, 3000 Sfax, Tunisie

(*Received 2 January 2012; in final form 6 February 2012*)

Two new noncentrosymmetric polar zinc sulfates have been synthesized by slow evaporation through the use of enantiomorphically pure sources of either (R)-2-methylpiperazine or (S)-2-methylpiperazine. A centrosymmetric analog was also prepared using a racemic source of the amine. The 3-D structure networks for these compounds consist of isolated $[Zn(H_2O)_6]^{2+}$, $[C_5H_{14}N_2]^{2+}$, and SO_4^{2-} linked by hydrogen bonds. The use of racemic 2-methylpiperazine results in crystallographic disorder of the amines and creation of inversion centers, while using a single enantiomer destroys the inversion symmetry and orders of the amines. These structures were determined using single-crystal X-ray diffraction, infrared spectroscopy, and thermal analyses. Crystal data are as follows: $[C_5H_{14}N_2][Zn(H_2O)_6](SO_4)_2$ (**1**), $a = 6.5988(1)$ Å, $b = 10.9613(2)$ Å, $c = 12.5479(2)$ Å, $\beta = 101.385(1)^\circ$, $V = 889.75(3)$ Å^3, $P2_1/n$ (No. 14), $Z = 2$; $[(R)\text{-}C_5H_{14}N_2][Zn(H_2O)_6](SO_4)_2$ (**2**), $a = 10.8665(2)$ Å, $b = 7.8600(1)$ Å, $c = 11.7029(2)$ Å, $\beta = 116.283(1)^\circ$, $V = 896.22(3)$ Å^3, $P2_1$ (No. 4), $Z = 2$; $[(S)\text{-}C_5H_{14}N_2][Zn(H_2O)_6](SO_4)_2$ (**3**), $a = 6.5819(2)$ Å, $b = 11.0014(2)$ Å, $c = 12.5229(3)$ Å, $\beta = 101.489(1)^\circ$, $V = 888.62(4)$ Å^3, $P2_1$ (No. 14), $Z = 2$.

Keywords: Noncentrosymmetric; Single enantiomer; Hydrogen bonds; Supramolecular structures; Thermal decomposition

1. Introduction

Inorganic–organic hybrid materials have undergone vast progress. Careful design of these materials can provide substances with unusual structural characteristics as well as extraordinary physical properties [1, 2]. Some simple cations, such as K^+, Rb^+, Cs^+, and NH_4^+, have been found to influence the structures of hybrid materials [3–5] and play significant roles in the assembly of molecular components. One approach has exploited organic amines where these simple cations are structure-directing agents [6, 7].

A host of organically templated metal sulfates have been reported [6, 8–13]. This mature system contains an exceptionally diverse range of organic–inorganic architectures and has yielded valuable information about formation mechanisms in such compounds [14]. We report the use of chiral organic amines to direct crystallographic noncentrosymmetry in a series of hexaaqua-zinc sulfates. The synthesis, structure, and

*Email: houcine_naili@yahoo.com

ISSN 0095-8972 print/ISSN 1029-0389 online
http://dx.doi.org/10.1080/00958972.2012.669476

characterization of three organically templated zinc sulfates are reported. $[Zn(H_2O)]^{2+}$ and SO_4^{2-} are observed in each compound. $[C_5H_{14}N_2][Zn(H_2O)_6](SO_4)_2$ (**1**) was synthesized using racemic 2-methylpiperazine and is centrosymmetric, while the noncentrosymmetric compounds $[(R)\text{-}C_5H_{14}N_2][Zn(H_2O)_6](SO_4)_2$ (**2**) and $[(S)\text{-}C_5H_{14}N_2][Zn(H_2O)_6](SO_4)_2$ (**3**) were synthesized using enantiomerically pure sources of (R)-2-methylpiperazine and (S)-2-methylpiperazine, respectively. Thermal decomposition shows crystalline anhydrous phases upon dehydration.

2. Experimental

2.1. *Materials*

$ZnSO_4 \cdot 7H_2O$ (98%), H_2SO_4 (96%), 2-methylpiperazine (95%, 2-mpip), (R)-(−)-2-methylpiperazine (97%, R-2-mpip), and (S)-(+)-2-methylpiperazine (99%, S-2-mpip) were purchased from Aldrich and used as received. Deionized water was used in these syntheses.

2.2. *Synthesis*

Compounds **1**–**3** were synthesized using a "slow evaporation" procedure of an aqueous solution. The clear solutions were stirred 15 min and allowed to stand at room temperature. After a few days, single crystals were formed. Reaction yields ranged between 60% and 70% based upon zinc. The products were filtered and washed with a small amount of distilled water.

2.2.1. $[C_5H_{14}N_2][Zn(H_2O)_6](SO_4)_2$ (1). Compound **1** was synthesized through reaction of 0.2875 g (1.00×10^{-3} mol) of $ZnSO_4 \cdot 7H_2O$, 0.1000 g (1.00×10^{-3} mol) of 2-mpip, 0.1962 g (2.00×10^{-3} mol) of H_2SO_4, and 4.9860 g (2.77×10^{-1} mol) of deionized water. White prismatic crystals were produced. IR data (cm^{-1}): N–H 1451, 1634; C–H 3012; S–O 1098, 1110; O–H 3344.

2.2.2. $[(R)\text{-}C_5H_{14}N_2][Zn(H_2O)_6](SO_4)_2$ (2). Compound **2** was synthesized through reaction of 0.2875 g (1.00×10^{-3} mol) of $ZnSO_4 \cdot 7H_2O$, 0.3000 g (3.00×10^{-3} mol) of R-2-mpip, 0.2943 g (3.00×10^{-3} mol) of H_2SO_4, and 4.9140 g (2.73×10^{-1} mol) of deionized water. White prismatic crystals were produced. IR data (cm^{-1}): N–H 1466, 1501; C–H 3012; S–O 1093, 1201; O–H 3411.

2.2.3. $[(S)\text{-}C_5H_{14}N_2][Zn(H_2O)_6](SO_4)_2$ (3). Compound **3** was synthesized through reaction of 0.2875 g (1.00×10^{-3} mol) of $ZnSO_4 \cdot 7H_2O$, 0.3000 g (3.00×10^{-3} mol) of S-2-mpip, 0.2943 g (3.00×10^{-3} mol) of H_2SO_4, and 4.9860 g (2.77×10^{-1} mol) of deionized water. White prismatic crystals were produced. IR data (cm^{-1}): N–H 1462, 1509; C–H 3020; S–O 1098, 1207; O–H 3415.

2.3. *Single-crystal X-ray diffraction*

The X-ray diffraction data were collected on a Nonius Kappa CCD, Bruker Smart Apex II diffractometer using Mo-Kα radiation ($\lambda = 0.71073$ Å). Single crystals were mounted on a glass fiber. Intensity data sets were collected through the program COLLECT [15]. Corrections for Lorentz-polarization effect, peak integration, and background determination were carried out with the program DENZO [16]. Frame scaling and unit cell parameter refinement were performed with the program SCALEPACK [16]. Analytical absorption corrections were performed by modeling the crystal faces [17]. The heavy atom positions were determined using SIR-92 [18]. All other non-hydrogen sites were located from Fourier difference maps. All non-hydrogen sites were refined using anisotropic thermal parameters using the full-matrix least-squares procedures on F_o^2 with $I > 3\sigma(I)$. The water hydrogen atoms were located in a difference map and refined with O–H distance restraints of 0.85(2) Å and H···H restraints of 1.39(2) Å so that the H–O–H angle fitted to the ideal value of a tetrahedron. Hydrogen atoms bonded to C and N were placed in geometrically idealized positions. Relevant crystallographic data are listed in table 1. Selected bond distances are presented in table 2.

Table 1. Crystallographic data for **1–3**.

Compound	**1**	**2**	**3**
Empirical formula	$C_5H_{26}ZnN_2O_{14}S_2$	$C_5H_{26}ZnN_2O_{14}S_2$	$C_5H_{26}ZnN_2O_{14}S_2$
Formula weight	467.77	467.77	467.77
Temperature (K)	293(2)	293(2)	293(2)
Wavelength (Å)	0.71073	0.71073	0.71073
Space group	$P2_1/n$ (No. 14)	$P2_1$ (No. 4)	$P2_1$ (No. 4)
Unit cell dimensions (Å, °)			
a	6.5988(1)	10.8665(2)	6.5819(2)
b	10.9613(2)	7.8600(1)	11.0014(2)
c	12.5479(2)	11.7029(2)	12.5229(3)
β	101.3850(1)	116.2830(1)	101.4890(1)
Volume (Å^3), Z	889.75(3), 2	896.22(3), 2	888.62(4), 2
Calculated density (g cm^{-3})	1.746	1.733	1.748
Absorption coefficient (mm^{-1})	1.684	1.672	1.686
Flack parameter	–	−0.028(9)	−0.015(11)
R_1[a]	0.0446	0.0302	0.0354
wR_2[b]	0.1232	0.0775	0.0965

[a] $R_1 = \Sigma\|F_o| - |F_c\|/\Sigma|F_o|$; [b] $wR_2 = [\Sigma w(F_o^2 - F_c^2)^2]/[\Sigma w(F_o^2)^2]^{1/2}$.

Table 2. Selected bond lengths (Å) in **1–3**.

Compound	**1**	**2**	**3**
Zn–Ow1	2.066(2)	2.086(2)	2.058(2)
Zn–Ow2	2.066(2)$^{\#1}$	2.098(2)	2.107(3)
Zn–Ow3	2.111(1)	2.113(2)	2.122(3)
Zn–Ow4	2.111(1)$^{\#1}$	2.103(2)	2.111(3)
Zn–Ow5	2.117(2)	2.081(2)	2.071(2)
Zn–Ow6	2.117(2)$^{\#1}$	2.105(2)	2.099(3)

Symmetry transformations used to generate equivalent atoms: $^{\#1}$ $-x, -y, -z$.

2.4. *IR spectroscopy*

Infrared (IR) measurements were obtained using a Perkin-Elmer FT-IR Spectrum from 400 to 4000 cm^{-1}. Samples were diluted with spectroscopic grade KBr and pressed into pellets.

2.5. *Thermal analyses*

Differential thermal analyses-thermogravimetric (DTA-TG) investigations were performed using a "multi-module 92 SETARAM" analyser operating from room temperature to 1000°C at a constant rate of 5°C min^{-1} under flowing air.

2.6. *Powder X-ray diffraction*

Temperature-dependent X-ray diffractions (TDXD) for **1** and **3** were performed with a D5005 powder diffractometer (Bruker AXS) using Cu-Kα radiation [$\lambda(K\alpha_1) = 1.5406$ Å, $\lambda(K\alpha_2) = 1.5444$ Å] selected with a diffracted-beam graphite monochromator and equipped with an Anton Paar HTK1200 high-temperature oven camera. Powder X-ray diffraction was used to support the structure determination and to identify the crystalline phases of **1**–**3**. The thermal decompositions of **1** and **3** were carried out in air with a heating rate of 7°C h^{-1} from ambient to 600°C. Temperature calibration was carried out with standard materials in the involved temperature range.

3. Results

$[C_5H_{14}N_2][Zn(H_2O)_6](SO_4)_2$ (**1**), $[(R)\text{-}C_5H_{14}N_2][Zn(H_2O)_6](SO_4)_2$ (**2**), and $[(S)\text{-}C_5H_{14}N_2][Zn(H_2O)_6](SO_4)_2$ (**3**) are constructed from octahedral metal cations coordinated by six water molecules, $[Zn(H_2O)_6]^{2+}$, isolated sulfates, $(SO_4)^{2-}$, and organic cations, all held together through extensive hydrogen-bonding networks. Zn–O_w bond lengths range between 2.066(2)–2.117(2) Å, 2.081(2)–2.113(2) Å, and 2.058(2)–2.122(3) Å for **1**, **2**, and **3**, respectively. These values are in agreement with values calculated from the bond valence program VALENCE [19] for a six-fold oxygen coordinated Zn^{II}, 2.109(2) Å and 2.113(2) Å in **1**, **2**, and **3**, respectively.

The structures of **1**–**3** are closely related. Indeed, the asymmetric units in each compound consist of either racemic or chiral sources of 2-methylpiperazinediium, SO_4^{2-} and one Zn^{II} cation octahedrally coordinated by six water molecules, similar to the well-known Tutton's salt, $A_2M(H_2O)_6(XO_4)_2$ (A = monovalent cation, M = bivalent cation, X = hexavalent cation) [20–23]. However, their symmetries differ greatly. Compound **1**, which was synthesized using racemic 2-mpip, crystallizes in the centrosymmetric space group $P2_1/n$ (No. 14). In contrast, **2** and **3** crystallize in the noncentrosymmetric polar space group $P2_1$ (No. 4). The primary differences between **2** and **3** are the presence of only R-2-mpip in **2** and only S-2-mpip in **3** and in the molecular arrangement. The 3-D packing of **1** is shown in figure 1, while packing images of **2** and **3** are depicted in figures 2 and 3, respectively.

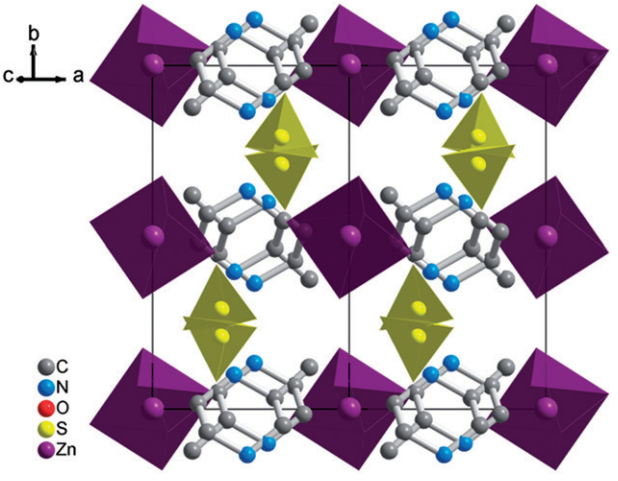

Figure 1. 3-D packing in **1**. The unit cell is shown. Hydrogen atoms have been removed for clarity.

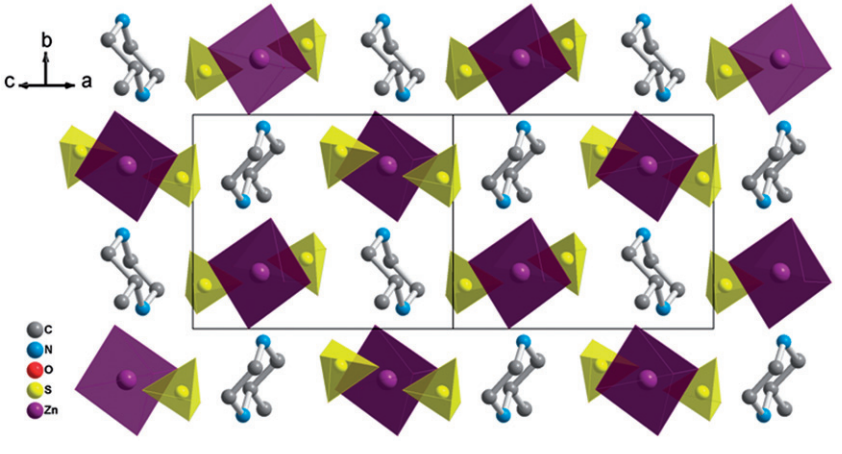

Figure 2. 3-D packing in **2**. Hydrogen atoms have been removed for clarity.

Compound **1** is isostructural with the related cobalt and manganese [24] phases. The metal cations are located in special positions on crystallographic inversion centers and each coordinated by six water molecules of which three are crystallographically independent. These $[Zn(H_2O)]^{2+}$ octahedra are slightly distorted. Bond angles of O–Zn–O fall in the range 86.15(6)–93.85(3)°, again analogous with other organically templated metal sulfates [20–23]. The $Zn(Ow)_6$ octahedra are isolated with shortest distance $Zn \cdots Zn = 6.599(2)$ Å, which are shorter than those found in related Mn and Co analogs [12, 13, 24–26]. The 2-methylpiperazinediiums are located about crystallographic inversion centers, with all atoms located in general positions. In the structure, a single disordered $[C_5H_{14}N_2]^{2+}$ was observed with two orientations of both $[R\text{-}C_5H_{14}N_2]^{2+}$ and $[S\text{-}C_5H_{14}N_2]^{2+}$ enantiomers. The carbons and nitrogen atoms are distributed between two positions related by the symmetry center with a refined site

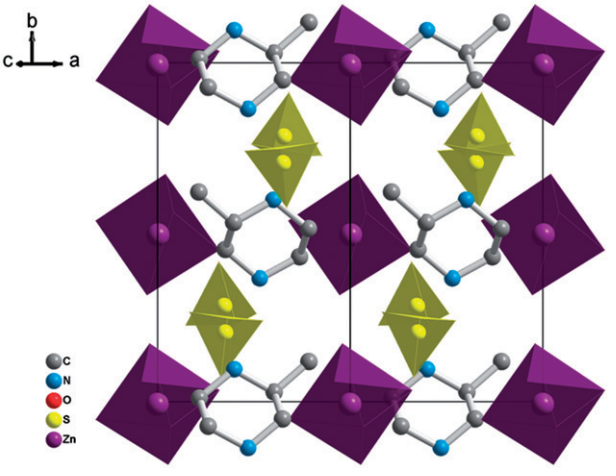

Figure 3. 3-D packing in **3**. Hydrogen atoms have been removed for clarity.

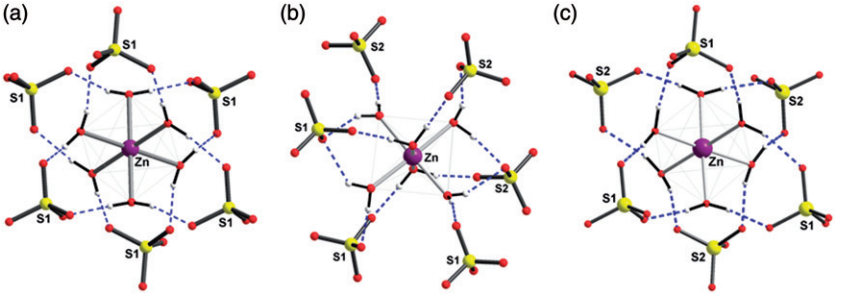

Figure 4. Neighboring sulfates in the environment of $[Zn(H_2O)_6]$ in **1** (a), **2** (b), and **3** (c).

occupancy factor equal to 0.5. For **1**, the N–C distances and the C–N–C angles range from 1.475(7) to 1.508(6) Å and from 111.7(4) to 112.2(4)°. These values are in agreement with those found in related amine complexes [21, 27, 28]. The sulfates are stacked such that they form anionic layers parallel to the cationic ones and play an important role in stability of the crystal structure by linking organic and inorganic cations *via* O_w–$H_w \cdots O$ and N–H$\cdots$O hydrogen bonds. The arrangement is an alternation of cationic and anionic layers along [101]. Hydrogen bonds are fairly strong, with donor–acceptor distances between 2.560(4) and 2.841(5) Å in O_w–$H_w \cdots O$ and between 2.664(2) and 2.910(3) Å in N–H$\cdots$O. Each Zn^{II} octahedron is surrounded by six sulfates H-bonded in a bidentate manner. Figure 4(a) shows neighboring sulfates in the environment of **1**.

Strong similarities in both structures are observed in **2** and **3**. These two materials crystallize in the noncentrosymmetric space group $P2_1$ (No. 4), for which the only symmetry elements are a series of 2_1 screw axes. However, despite the similarities in compositions in **2** and **3**, distinct differences in 3-D packing are observed. The Flack parameters refined to −0.028(9) and −0.015(11) for **2** and **3**, indicating absolute

configurations. The enantiomeric structures are inverses of one another and are isostructural with related metal phases [26]. The local coordination environments around $[Zn(H_2O)_6]^{2+}$ in **2** and **3** are shown in figures 2 and 3. The octahedra of Zn^{II} cations are not regular (table 2), as seen in other isostructural metal sulfates [29]. The *cis*-O–Zn–O angles range from 85.05(8)° to 94.80(7)° in **1** and between 85.87(1)° and 95.61(1)° in **2**, while the *trans*-O–Zn–O angles deviate from the ideal value by approximately 3° for **2** and **3**, respectively.

In **2** and **3**, the $[Zn(H_2O)_6]^{2+}$ cations are separated through two short, four intermediate and four long distances, with approximate values of 5.359×2, 6.582×2, 7.063×2, 7.860×2, 10.862×4 Å. These $M^{II} \cdots M^{II}$ distances are both shorter and longer than analogous phases containing other diammonium cations, 7.303 Å for $[diazabicyclo[2.2.2]octaneH_2]^{2+}$ [13, 21], 6.544 Å for $[piperazineH_2]^{2+}$ [12, 29], and 8.095 Å for $[1,4\text{-}butanediamineH_2]^{2+}$ [30]. The trend in these distances mirrors the sizes of the included organic cations.

$[Zn(H_2O)_6]^{2+}$ stack along the [101] directions in **2** and form inorganic pseudolayers with the $(SO_4)^{2-}$ in the *bc*-plane. $[Zn(H_2O)_6]^{2+}$ in **2** is surrounded by two monodentate, two bidentate, and two tridentate SO_4^{2-} anions, as shown in figure 4(b). The geometries of these interactions differ from **1** and **3**, as each $[Zn(H_2O)_6]^{2+}$ donates hydrogen bonds to six adjacent SO_4^{2-} tetrahedra in a bidentate manner. As in **2**, the organic cations also donate hydrogen bonds to neighboring SO_4^{2-} tetrahedra. The N–H $\cdots$ O distances range between 2.737(3) and 2.913(3) Å, while the O_w–H $\cdots$ O distances range between 2.664(2) and 2.819(3) Å. These values agree with those currently observed in inorganic salts containing the organic groups [9, 26]. Extended, supramolecular structures are constructed from these molecular units by hydrogen-bonding. While **3** contains $[Zn(H_2O)_6]^{2+}$ cations stacked along the [101], [100], and [010] directions and are separated by SO_4^{2-} and $[S\text{-}C_5H_{14}N_2]^{2+}$ (figure 4c). Each $[Zn(H_2O)_6]^{2+}$ cation donates hydrogen bonds to six adjacent SO_4^{2-} groups, each of which accepts hydrogen bonds from at least two H_2O ligands on the same Zn. The $[S\text{-}C_5H_{14}N_2]^{2+}$ cations also donate hydrogen bonds to nearby SO_4^{2-} groups, creating an extended, supramolecular structure. The cation–anion distances range between 2.673(3) and 2.804(4) Å for N–H $\cdots$ O interactions and between 2.670(4) and 2.983(4) Å for O_w–H $\cdots$ O interactions.

4. Thermal decomposition

Thermal properties of **1** and **3** were probed using TG, DTA, and 3-D representation of the powder diffraction patterns (TDXD) obtained under flowing air (figures 5 and 6). Thermal decompositions of the compounds are complex and take place in several steps.

Figure 5(a) shows the TG-DTA curves obtained during decomposition of $[C_5H_{14}N_2][Zn(H_2O)_6](SO_4)_2$ from 20°C to 900°C. The TG curve shows that the dehydration occurs between 50°C and 150°C and corresponds to loss of six water molecules (observed and theoretical weight losses, 23.51% and 23.08%). This is accompanied with an endothermic peak on the DTA curve, at 118°C. The TDXD plot (figure 5b) reveals that the precursor is stable until 120°C and then transforms into the anhydrous phase, $[C_5H_{14}N_2]Cu(SO_4)_2$ (crystalline phase Cr). Decomposition of the anhydrous compound starts at 300°C and leads to a mixture of crystalline $Zn_3O(SO_4)_2$ and ZnO (PDF no. 01-071-2475). This transformation is accompanied, on the DTA

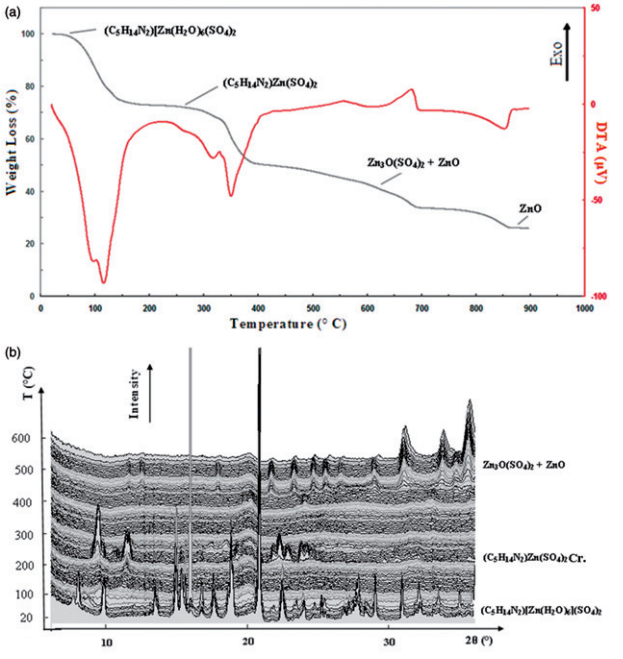

Figure 5. (a) DTA-TG curves of thermal decomposition of $[C_5H_{14}N_2][Zn(H_2O)_6](SO_4)_2$ (**1**), and (b) TDXD plot for the decomposition of $[C_5H_{14}N_2][Zn(H_2O)_6](SO_4)_2$ (**1**).

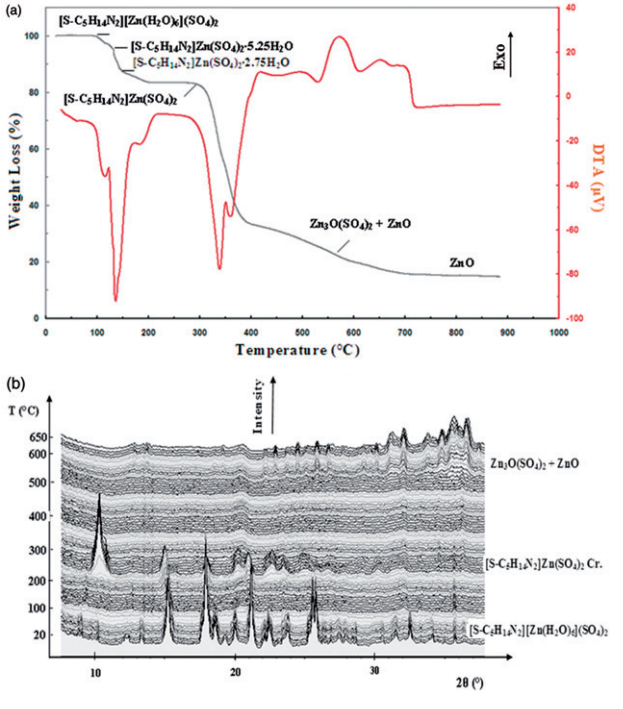

Figure 6. (a) DTA-TG curves of thermal decomposition of $[S\text{-}C_5H_{14}N_2][Zn(H_2O)_6](SO_4)_2$ (**3**), and (b) TDXD plot for the decomposition of $[C_5H_{14}N_2][Zn(H_2O)_6](SO_4)_2$ (**3**).

curve, by two endothermic peaks observed at 305°C and 350°C, respectively. The last transformation starts at 690°C and corresponds to total decomposition of $Zn_3O(SO_4)_2$ into ZnO (PDF no. 00-036-1451) (observed weight loss, 83.21%; calculated weight loss, 82.61%).

Figure 6(a) and (b) shows successive weight losses for **3**. Dehydration of $[S\text{-}C_5H_{14}N_2][Zn(H_2O)_6](SO_4)_2$ occurs in three stages. First, a weight loss of 2.52% at 95°C corresponds to the departure of 0.75 H_2O (theoretical weight loss, 2.88%). The second stage of the dehydration takes place between 127°C and 150°C and corresponds to loss of 2.5 H_2O (observed weight loss, 9.43%; calculated weight loss, 9.62%). The third transformation starts at ~152°C and corresponds to loss of the last 2.75 water molecules (observed weight loss, 9.98%; calculated weight loss, 10.58%), leading to the anhydrous phase $[S\text{-}C_5H_{14}N_2]Zn(SO_4)_2$. These phenomena are accompanied by three endothermic peaks on the DTA curve, maximum at 195°C. The TDXD plot shows that $[S\text{-}C_5H_{14}N_2]Zn(SO_4)_2$ is a crystalline phase. The decomposition of the anhydrous phase starts near 310°C, includes loss of the organic moiety, and leads to a mixture of crystalline $Zn_3O(SO_4)_2$ and ZnO (PDF no. 01-071-2475). This transformation is accompanied, on the DTA curve, by two endothermic peaks observed at 330°C and 360°C, respectively. The last stage corresponds to the total decomposition of the zinc sulfate, starting at about 700°C, and gives zinc oxide ZnO.

5. Discussion

Compounds **1**–**3** were obtained by slow evaporation of solutions containing either racemic or chiral diamine. Initial studies were conducted using a racemic source of the amine 2-mpip, from which **1** was formed. Subsequent reactions focused on studying the effects of using enantiomorphically pure sources of either R-2-mpip or S-2-mpip. As noted above, use of chiral organic amines favors formation of new noncentrosymmetric materials [26, 31–34]. However, the progression from syntheses using racemic to enantiomorphically pure chiral amines is complex. The role of crystallographic order and disorder must be addressed.

The molecule 2-mpip was selected for this study because this rigid diamine is not likely to exhibit orientational disorder, owing to its low molecular flexibility and multiple points of interaction between each cation and the inorganic components. Despite this, only one disorder mechanism is observed in $[C_5H_{14}N_2]^{2+}$ in **1**. Inversion symmetry within the cations results in superimposition of both $[R\text{-}C_5H_{14}N_2]^{2+}$ and $[S\text{-}C_5H_{14}N_2]^{2+}$ (figure 7). Such disorder is found in the related manganese and cobalt phases [24]. The use of a single enantiomer destroys these centers of symmetry and crystallographically orders the cations. The elimination of this inversion symmetry results in ordering of all $[C_5H_{14}N_2]^{2+}$ cations in **2** and **3** and forces a reduction in symmetry from $P2_1$.

The possibility of pseudosymmetry in **2** and **3** was investigated. The organic cations were removed from the crystallographic models and PLATON [35] was used to probe for missing symmetry. The ADDSYM command suggests the possibility of a missing additional symmetry leading to the $P2_1/c$ space group (No. 14), with inversion symmetry directly between the metal centers. The position of the methyl groups on the 2-methylpiperazinediium cation rings violates the pseudosymmetry found by PLATON,

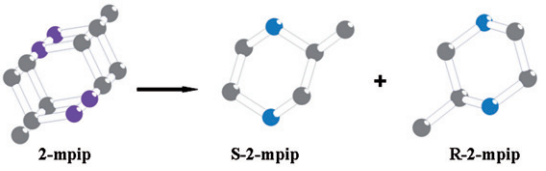

Figure 7. Disorder mechanism present in the $[2\text{-mpipH}_2]^{2+}$ cations in **1**.

and does not recognize the contribution of a single $-CH_3$ group over the rest of the structure. In addition, the systematic absences are not correct for $P2_1/c$. Specifically, the expected $l = 2n + 1$ absences in $h0l$ reflections are not present. These results confirm the crystallographic noncentrosymmetry in **2** and **3**.

Counterpoints to the role of template disorder in **1** can be found in related systems based upon the templated copper sulfate compound $[C_5H_{14}N_2][Cu(H_2O)_4](SO_4)_2 \cdot H_2O$ [11], which was synthesized using the same amine under slow evaporation conditions and crystallized in the centrosymmetric space group $P2_1/n$ (No. 14). A single $[C_5H_{14}N_2]^{2+}$ is present in the asymmetric unit, while both $[R\text{-}C_5H_{14}N_2]^{2+}$ and $[S\text{-}C_5H_{14}N_2]^{2+}$ cations are generated through a series of inversion centers in the structure. Identical syntheses using either enantiomorphic R-2-mpip or S-2-mpip result in the noncentrosymmetric compounds [9, 31].

The three systems presented above display similarities and differences. The use of a racemic 2-mpip results in disordered $[C_5H_{14}N_2]^{2+}$ cations in **1**, ordered $[R\text{-}C_5H_{14}N_2]^{2+}$, and $[S\text{-}C_5H_{14}N_2]^{2+}$ cations in $[C_5H_{14}N_2][Cu(H_2O)_4](SO_4)_2 \cdot H_2O$. However, the use of enantiomorphically pure sources of 2-mpip in **2** and **3** directs crystallization to noncentrosymmetric space groups and crystallographically orders the organic cations.

The thermal analysis (DTA-TG and TDXD) curves for **1** and **3** show that there are similar changes in the decomposition of precursors with small differences, which could be associated with the difference of dehydration temperatures.

6. Concluding remarks

Directed synthesis of noncentrosymmetric zinc sulfates is possible through incorporation of enantiomerically pure chiral amines. Despite the presence of crystallographic disorder when using a racemic source of the amine, syntheses containing either R-2-mpip or S-2-mpip result in two new noncentrosymmetric hybrid compounds. Thermal analyses studied by TG-DTA and TDXD for **1** and **3** show that there are similar changes in decomposition of precursors with somewhat small differences, which could be associated with the structural variations. Specifically, dehydration temperatures are affected by both the strengths and topologies of the extensive hydrogen-bonding structures.

Supplementary material

Crystallographic data (excluding structure factors) for the structures reported in this article have been deposited with the Cambridge Crystallographic Data Center as

supplementary publication Nos CCDC 859888–859890. Tables of hydrogen-bond details for all compounds are available in the Supplementary material.

Acknowledgments

Sincere thanks are expressed to Dr T. Roisnel (Centre de Diffractométrie X, Université de Rennes I) for the assistance in single-crystal X-ray diffraction data collection.

References

[1] O.R. Evans, W.B. Lin. *Acc. Chem. Res.*, **35**, 511 (2002).
[2] D.W. Breck. *Zeolite Molecular Sieves: Structure, Chemistry and Use*, Wiley & Sons, London (1974); A. Clearfield. *Chem. Rev.*, **88**, 125 (1988); P.B. Venuto. *Microporous Mater.*, **2**, 297 (1994).
[3] P. Naumov, V. Jordanovska, M.G.B. Drew, S.W. Ng. *Solid State Sci.*, **4**, 455 (2002).
[4] H. Euler, B. Barbier, A. Meents, A. Kirfel. *Z. Kristallogr.*, **218**, 265 (2003).
[5] L.V. Soboleva, L.F. Kirpichnikova. *Crystallogr. Rep.*, **46**, 306 (2001).
[6] A.K. Cheetham, G. Ferey, T. Loiseau. *Angew. Chem. Int. Ed. Engl.*, **38**, 3268 (1999).
[7] R.C. Haushalter, L.A. Mundi. *Chem. Mater.*, **4**, 31 (1992).
[8] L.F. Kirpichnikova, L.A. Shuvalov, N.R. Ivanov, B.N. Prasolov, E.F. Andreyev. *Ferroelectrics*, **96**, 313 (1989).
[9] F. Hajlaoui, S. Yahyaoui, H. Naïli, T. Mhiri, T. Bataille. *Inorg. Chim. Acta*, **363**, 691 (2010).
[10] H. Naïli, W. Rekik, T. Bataille, T. Mhiri. *Polyhedron*, **25**, 3543 (2006).
[11] F. Hajlaoui, S. Yahyaoui, H. Naïli, T. Mhiri, T. Bataille. *Polyhedron*, **28**, 2113 (2009).
[12] W. Rekik, H. Naïli, T. Bataille, T. Roisnel, T. Mhiri. *Inorg. Chim. Acta*, **359**, 3954 (2006).
[13] W. Rekik, H. Naïli, T. Bataille, T. Mhiri. *J. Organomet. Chem.*, **691**, 4725 (2006).
[14] L. Carlucci, G. Ciani, D.M. Proserpio. *Chem. Commun.*, 380 (2004).
[15] Nonius. Data Collection Software for Nonius Kappa-CCD devices. Nonius BV, Delft, The Netherlands (2001a).
[16] Z. Otwinowski, W. Minor, C.W. Carter, R.M. Sweet. *Methods in Enzymology*, Vol. 276, p. 307, Academic Press, New York (1997).
[17] J. de Meulenaer, H. Tompa. *Acta Crystallogr.*, **19**, 1014 (1965).
[18] A. Altomare, G. Cascarano, C. Giacovazzo, A.J. Guagliardi. *Appl. Crystallogr.*, **26**, 343 (1993).
[19] I.D. Brown. *J. Appl. Cryst.*, **29**, 479 (1996).
[20] P. Held. *Acta Crystallogr.*, **E59**, m197 (2003).
[21] S. Yahyaoui, W. Rekik, H. Naïli, T. Mhiri, T. Bataille. *J. Solid State Chem.*, **180**, 3560 (2007).
[22] T. Bataille. *Acta Crystallogr.*, **C59**, m459 (2003).
[23] M. Fleck, L. Bohaty, E. Tillmanns. *Solid State Sci.*, **6**, 469 (2004).
[24] F. Hajlaoui, H. Naïli, S. Yahyaoui, M.M. Turnbull, T. Mhiri, T. Bataille. *Dalton Trans.*, 11613 (2011).
[25] W. Rekik, H. Naili, T. Mhiri, T. Bataille. *Mater. Res. Bull.*, **43**, 2709 (2008).
[26] F. Hajlaoui, H. Naïli, S. Yahyaoui, A.J. Norquist, T. Mhiri, T. Bataille. *J. Organomet. Chem.*, **700**, 110 (2012).
[27] S.J. Choyke, S.M. Blau, A.A. Larner, A.N. Sarjeant, J. Yeon, P.S. Halasyamani, A.J. Norquist. *Inorg. Chem.*, **48**, 11277 (2009).
[28] E.A. Muller, R.J. Cannon, A.N. Sarjeant, K.M. Ok, P.S. Halasyamani, A.J. Norquist. *Cryst. Growth Des.*, **5**, 1913 (2005).
[29] W. Rekik, H. Naili, T. Mhiri, T. Bataille. *Acta Cryst.*, **E61**, m629 (2005).
[30] W. Rekik, H. Naïli, T. Mhiri, T. Bataille. *Solid State Sci.*, **11**, 614 (2009).
[31] F. Hajlaoui, S. Yahyaoui, H. Naïli, T. Mhiri, T. Bataille. *J. Struct. Chem.*, **53**, 359 (2012).
[32] D.J. Hubbard, A.R. Johnston, H. Sanchez Casalongue, A.N. Sarjeant, A.J. Norquist. *Inorg. Chem.*, **47**, 8518 (2008).
[33] J.R. Gutnick, E.A. Muller, A.N. Sarjeant, A.J. Norquist. *Inorg. Chem.*, **43**, 6528 (2004).
[34] T.R. Veltman, A.K. Stover, A.N. Sarjeant, K.M. Ok, P.S. Halasyamani, A.J. Norquist. *Inorg. Chem.*, **45**, 5529 (2006).
[35] A.L.J. Spek. *Appl. Crystallogr.*, **36**, 7 (2003).